Journal of Physical Chemistry and Functional Materials

Home Page of Journal: https://dergipark.org.tr/jphcfum

Quercetin and Gallic Acid containing Hydroxyapatites: Synthesis and Characterization

Tankut Ates [a,*], Serhat Keser [b], Suleyman Koytepe [c], Niyazi Bulut [d], Omer Kaygili [d]

[a] *Department of Engineering Basic Sciences, Faculty of Engineering and Natural Sciences, Malatya Turgut Özal University, Battalgazi, Malatya, Türkiye*
[b] *Department of Chemical Technology, EOSB Higher Vocational School, Firat University, Elazig, Türkiye*
[c] *Department of Chemistry, Faculty of Arts and Science, Inonu University, Malatya, Türkiye*
[d] *Department of Physics, Faculty of Science, Firat University, Elazig, Türkiye*
** Corresponding author: E-mail: tankut.ates@ozal.edu.tr*

ABSTRACT

In the present study, hydroxyapatite (HAp) samples containing gallic acid or quercetin were synthesized using the wet chemical method. The synthesized samples were examined to ascertain the impact of gallic acid and quercetin incorporation on the structural and thermal characteristics of HAp. The samples were investigated using X-ray diffraction (XRD), Fourier transform infrared (FTIR), thermogravimetric analysis (TGA), differential thermal analysis (DTA), scanning electron microscopy (SEM), and energy dispersive X-ray (EDX) spectroscopy. The XRD and FTIR results corroborate the formation of the HAp phase. It was observed that the addition of gallic acid and quercetin used in the synthesis had effects on the morphology, unit cell parameters, degree of crystallinity, and crystallite size. Additionally, the thermal analysis results indicate that gallic acid and quercetin exert a considerable influence on the thermal behavior of HAp.

ARTICLE INFO

Keywords:
Hydroxyapatite,
Quercetin,
Gallic acid,
X-ray diffraction,
Scanning electron microscopy

Received: 2024-09-05
Accepted: 2024-10-02
ISSN: 2651-3080
DOI: **10.54565/jphcfum.1544293**

1. Introduction

The pursuit of innovative biomaterials that mimic the structure of natural tissues and can facilitate the body's healing processes has remained of significant importance for many years [1]. Among the various types of biomaterials, bioceramics have been widely utilized in medical engineering as fillers and regeneration agents for bone tissues [2]. Among bioceramics, an intriguing material is hydroxyapatite (HAp), a member of the calcium phosphate (CaP) family, with the chemical formula of $Ca_{10}(PO_4)_6(OH)_2$. HAp materials have a Ca/P atomic ratio between 1.5 and 1.67 [3].

HAp demonstrates excellent biocompatibility, bioactivity, osteoconductive, osteoinductive, and osteointegrative properties, biodegradability, and non-immunogenic behavior [1-6]. Consequently, HAp has long been considered an exceptional candidate for various biomedical applications, including tissue engineering, orthopedics, dentistry, and imaging [1,3-4,7]. In addition to being recognized as a reference material for hard tissue applications, it has recently been employed in soft tissue regeneration with antibacterial capabilities. HAp can be used as a drug carrier due to its ability to bind various drugs and biological molecules [4]. Since HAp bioceramics are inherently brittle and exhibit lower fracture toughness compared to natural bone, their applications in orthopedics are generally confined to non-load-bearing implants, filling bone defects, or as coatings in dense or porous forms [3,8].

Various preparation techniques such as sol-gel, solid-state, chemical precipitation, hydrothermal, mechanochemical-hydrothermal, wet chemical, spray pyrolysis, microwave, microemulsion, and combustion synthesis have been used for preparing HAp [2,7,9].

Song et al. [10], in their study emphasizing the efficacy of quercetin in bone regeneration, predicted that the synthesized quercetin (low-content)/silk fibroin/HAp scaffolds provided a biomimetic bone-like microenvironment, thereby proposing a potential alternative graft for high-performance bone tissue regeneration. Forte et al. [11] indicated that HAp could be functionalized with quercetin through different synthesis methods, noting that quercetin possesses pharmacological activities, antioxidant and anti-inflammatory properties, as well as the ability to prevent bone loss. Silva-Holguín et al. [12] reported that chemical synthesis using non-toxic acids such as gallic acid provides an eco-friendly, facile, and scalable method, successfully preparing HAp and Ag-doped HAp composites via the sol-gel and green chemical methods. They also observed that the synthesized composites exhibited significant antibacterial activity despite the low silver concentration. Tang et al. [13], in their investigation of the effects of gallic acid on the crystal growth of HAp, found that in the presence of gallic acid, the crystals tended to form spheroidal structures, and as the concentration of gallic acid increased, a reduction in crystal size was observed. Jerdioui et al. [14] noted that in nHAp-GA composites, gallic acid contributed to low crystallinity, small crystallite size, and exhibited antibacterial and anti-inflammatory properties.

This study is aimed to synthesize and investigate the effects of gallic acid and quercetin on the structural properties of HAp.

2. Material and Method

2.1. Synthesis

A total volume of 100 mL of 0.5 M calcium nitrate tetrahydrate (Carlo-Erba) was dissolved in the distilled water. In another flask, 0.3 M diammonium hydrogen phosphate was dissolved in the same solvent. The first solution was poured into a beaker, and then the second one was added drop wisely into the first solution. The pH values of all the final mixtures were adjusted to the value of 9.45 with the addition of ammonia solution (Sigma-Aldrich), and these mixtures were stirred at room temperature for 2.5 hours and then put into an oven at 150 ºC for 17 hours to dry. For the calcination, the samples in the form of the powder were heated in an electric furnace at 825 ºC for 2.5 hours. 0.1 M Gallic acid and 0.1 M Quercetin solutions were prepared by dissolving them separately in a suitable solvent. Gallic acid-HAp and Quercetin-HAp samples were mixed in a beaker with powdered samples taken from the oven and placed in an ultrasonic water bath. The samples were kept in an ultrasonic water bath at 65 ºC for 5 hours and left to dry in an oven at 130 ºC for 10 hours. Powdered samples were used for further analysis.

2.2. Characterization

X-ray diffraction (XRD) analysis was performed using a Bruker D8 Advance equipment using CuKα radiation in the 2θ range from 20° to 60° with a step of 0.02°. A PerkinElmer Spectrum One spectrophotometer was used to collect the Fourier transform infrared (FTIR) spectra of the samples using the KBr pellets in the wavenumber interval of 4000-400 cm^{-1} with a step of 4 cm^{-1}. Thermal measurements, containing differential thermal analysis (DTA), and thermogravimetric analysis (TGA), were conducted using Shimadzu's DTA-50 and TGA-50, devices, respectively from room temperature to 1000 °C at the heating rate of 10 °C/min. The morphological observations were carried out using an FEI Quanta 250 FEG scanning electron microscope (SEM) using an accelerating voltage of 15 keV at the magnification of 60,000X for each sample.

3. Results and Discussions

3.1. XRD analysis

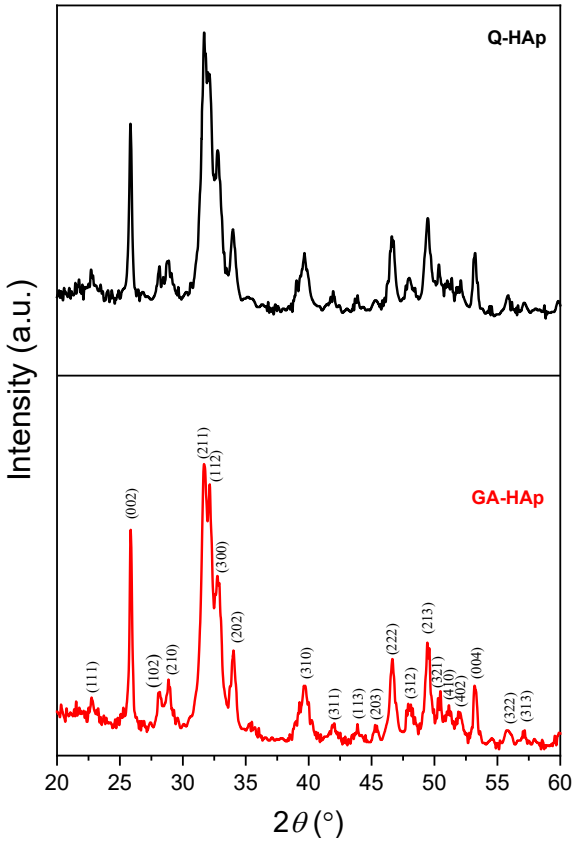

Fig. 1. XRD graphs of GA- and Q-containing HAps

XRD patterns obtained from the crystal phase analyses of HAp powders are presented in Figure 1, indicating a polycrystalline structure. The patterns indicate

the presence of the HAp phase (PDF No. 09-0432) [15] and do not reveal the presence of any secondary phases. It has been observed that the incorporation of GA and Q into the HAp structure induces alterations in the intensity and positions of the peaks in the patterns. The crystal size (D) and crystallinity percentage (X_C%) were determined using the Scherrer equation [6] and the relation provided by Landi et al. [16], respectively, as follows:

$$D = \frac{0.9\lambda}{\beta \cos\theta} \quad (1)$$

$$X_C\% = \left(1 - \frac{V_{112/300}}{I_{300}}\right) \times 100 \quad (2)$$

In this context, λ represents the wavelength, θ denotes the diffraction angle, β signifies the full width at half maximum, I_{300} is the intensity of the (300) peak, and $V_{112}/_{300}$ is the intensity of the trough between the (112) and (300) diffraction peaks. The estimated values of the parameters, which were calculated from the XRD patterns via an experimental process, are provided in Table 1. This table also highlights changes in these parameters. As illustrated in the table, the unit cell parameters demonstrate an increase with the incorporation of GA and Q content during the synthesis process.

Table 1. XRD analysis report

	HAp (JCPDS 09-0432)	GA-HAp	Q-HAp
D (nm)	-	30.66	27.00
Xc%	-	70.1	72.0
a (nm)	0.9418	0.9462	0.9467
c (nm)	0.6884	0.6885	0.6890
c/*a*	0.7309	0.7277	0.7278
V $(nm)^3$	0.5288	0.5338	0.5348

3.2. FTIR results

Fig. 2 presents the Fourier Transform Infrared (FT-IR) spectra of HAp samples synthesized using Gallic acid and Quercetin. In these spectra, bands associated with hydroxyl and phosphate groups were identified within the range of 4000–400 cm^{-1}. Among the bands related to the phosphate group, the asymmetric stretching vibration mode of the P-O bond was observed at 1090 and 1024 cm^{-1} for GA-HAp, while for Q-HAp, it was detected at 1089 and 1024 cm^{-1} [17,18]. The symmetric stretching mode of the P-O bond was observed at 962 cm^{-1} for both HAp samples [17,19], and the bending vibration mode of the O-P-O bond was detected at 601 and 561 cm^{-1} for both samples as well [17,20]. The bending mode for the phosphate group was identified at 472 cm^{-1} [17]. Regarding the hydroxyl group, the libration mode was positioned at 633 cm^{-1} for GA-HAp and at 632 cm^{-1} for Q-HAp, while the stretching mode was located at 3573 cm^{-1} for GA-HAp and at 3572 cm^{-1} for Q-HAp [17,21]. The bands of 2900 and 2980 cm^{-1} are associated with the vibrational mode of C-H bond due to quercetin ($C_{15}H_{10}O_7$) or gallic acid ($C_7H_6O_5$) contents in the samples [22].

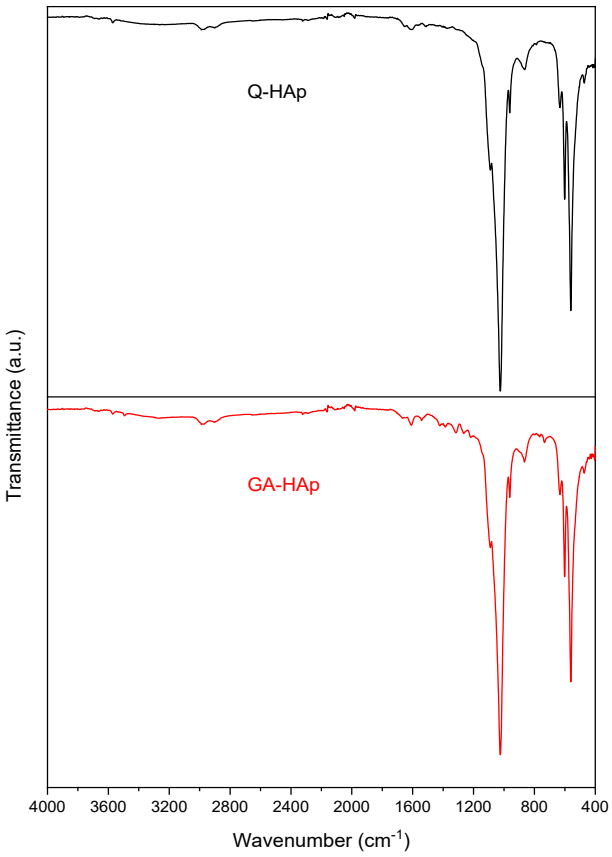

Fig. 2. FTIR results of the samples

3.3. Thermal characterization

The TGA and DTA thermograms of the Gallic acid-HAp and Quercetin-HAp samples are shown in Figure 3. In the DTA curves, an exothermic peak was observed at 263°C (weak) for the GA-HAp sample and 321°C (sharp) for the Q-HAp sample. These peaks can be associated with the removal of physically and/or chemically adsorbed water molecules [23,24]. A second exothermic peak in the DTA curves was detected at 900°C (sharp) and 892°C (weak) for the GA-HAp and Q-HAp samples, respectively. This peak is likely related to the decomposition of the samples and the initiation of β-TCP phase formation [25-27].

The TGA curves of the synthesized HAp samples showed weight loss with increasing temperature for all samples. The total weight losses up to 1000°C were found to be approximately 9.4% and 11.2%, respectively. The TGA curves revealed two major weight loss regions for both samples. The first weight loss region for the GA and Q containing samples was observed in the temperature range of 30-122°C and 32-122°C, respectively. This

weight loss may be attributed to the removal of adsorbed water from the surface and interparticle spaces [24]. The second and most significant weight loss region was observed in the temperature ranges of 172-459°C and 182-441°C for the GA and Q containing HAp structures, respectively. This second major weight loss is thought to result from the removal of chemically adsorbed water from the lattice structure, as well as the loss of organic residues and the crystallization of HAp [24,28]. İn addition to these, the mass losses can be due to the elimination of gallic acid and quercetin, as well as removal of the water, because the melting points of gallic acid and quercetin are about 260 and 316 °C, respectively. Finally, no significant weight loss was detected after 459°C and 441°C for these samples, respectively, indicating that the synthesized GA and Q-doped HAp structures are thermally stable at higher temperatures [28].

From the thermal analysis results, it can be concluded that Gallic acid and Quercetin significantly influence the thermal behavior of HAp.

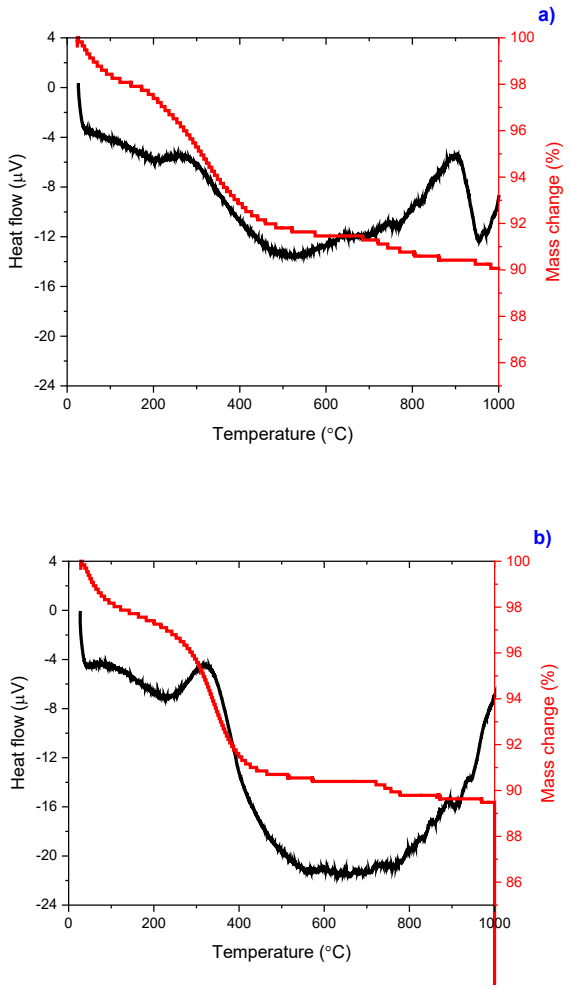

Fig. 3. DTA and TGA thermograms of **a)** the GA-HAp and **b)** Q-HAp samples from room temperature to 1000 °C

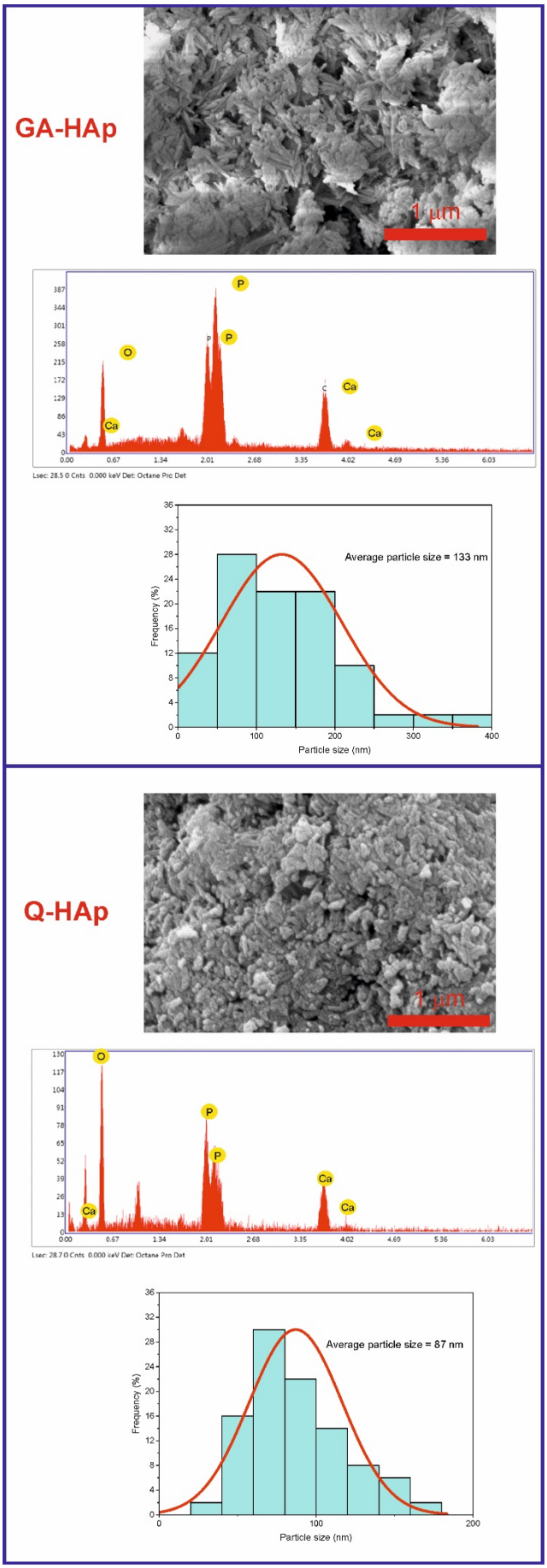

Fig. 4. Morphological investigation results of the samples

3.4. SEM observations

The SEM images taken at the magnification of X60,000 for all the samples are illustrated in Fig. 3. It is seen that all the samples are composed of smaller particles and the average particle sizes are found to be 133 nm for the GA-HAp and 87 nm for the Q-HAp. The GA-HAp sample is consisted of randomly-oriented nano-sized rods and the Q-HAp sample is composed of the stacked sphere-like nanoparticles. The EDX results verify that both samples contain the elements of Ca, P and O. There is no impurity is detected.

4. Discussion

The HAp samples were synthesized using the wet chemical method, with the same amount of gallic acid and quercetin being added separately. The impact of incorporating gallic acid and quercetin during the synthesis process on the structural, morphological, and thermal properties of hydroxyapatite was examined. It was observed that these organic compounds exerted a significant influence on the investigated properties of the HAp material. The unit cell parameters, as determined from the XRD results, exhibited an increase with the incorporation of GA and Q content during the synthesis process. The average particle size was determined to be 133 nm for GA-HAp and 87 nm for Q-HAp based on the findings of the morphological investigation. The FTIR results indicate that while the addition of GA and Q does not result in significant shifts in the positions of the bands, there are differences in their intensities.

Competing interests

The authors declare that they have no competing interests.

Acknowledgements

This work was supported by the Management Unit of Scientific Research Projects of Firat University (FUBAP) (Project Number: FF.24.22).

References

[1] R. Kumar, D. Shikha and S. K. Sinha. Antioxidant properties and thrombogenic evaluation of Copper-Manganese Alloy-Doped hydroxyapatite in comparison to un-doped hydroxyapatite. Inorganic Chemistry Communications. 2024;165: 112490. https://doi.org/10.1016/j.inoche.2024.112490.

[2] F. Hosseini, F. Soltanolkottabi, M. M. Behrouzfar and H. Jafari. Powder mixture of hydroxyapatite and tetracalcium phosphate for hard tissue applications. Moroccan Journal of Chemistry. 2024;12(2):534-553. https://doi.org/10.48317/IMIST.PRSM/morjchem-v12i2.40173.

[3] C. Tavares, T. Vieira, J. C. Silva, J. P. Borges and M. C. Lança. Bioactive Hydroxyapatite Aerogels with Piezoelectric Particles. Biomimetics. 2024;9(3):143. https://doi.org/10.3390/biomimetics9030143.

[4] H. Inam, S. Sprio, M. Tavoni, Z. Abbas, F. Pupilli and A. Tampieri. Magnetic hydroxyapatite nanoparticles in regenerative medicine and nanomedicine. International Journal of Molecular Sciences. 2024;25(5):2809. https://doi.org/10.3390/ijms25052809.

[5] T. Ates, S. V. Dorozhkin, O. Kaygili, M. Kom, I. Ercan, N Bulut, F. Firdolas, S. Keser, N. C. Gursoy, I. H. Ozercan, Y. Eroksuz, T. İnce. The effects of Mn and/or Ni dopants on the in vitro/in vivo performance, structural and magnetic properties of β-tricalcium phosphate bioceramics. Ceramics International. 2019;45(17):22752-22758. https://doi.org/10.1016/j.ceramint.2019.07.314.

[6] S. Acar, O. Kaygili, T. Ates, S. V. Dorozhkin, N. Bulut, B. Ates, S. Koytepe, F. Ercan, H. Kebiroglu, A. H. Hssain. Experimental characterization and theoretical investigation of Ce/Yb co-doped hydroxyapatites. Materials Chemistry and Physics. 2022;276:125444. https://doi.org/10.1016/j.matchemphys.2021.125444.

[7] D. Predoi, S. C. Ciobanu, S. L. Iconaru, Ş. Ţălu, L. Ghegoiu, R. S. Matos, H. D. da Fonseca Filho, R. Trusca. New Physico-Chemical Analysis of Magnesium-Doped Hydroxyapatite in Dextran Matrix Nanocomposites. Polymers. 2023;16(1):125. https://doi.org/10.3390/polym16010125.

[8] H. G. Ateş, O. Kaygili, N. Bulut, F. Osmanlıoğlu, S. Keser, B. Tatar, B. K. Mahmood, T. Ates, F. Ercan, I. Ercan, B. Ates and İ. Özcan. Investigation of the structural, thermal, magnetic and cell viability properties of Ce/Sr co-doped hydroxyapatites. Journal of Molecular Structure. 2023;1283:135318. https://doi.org/10.1016/j.molstruc.2023.135318.

[9] O. Kaygili, S. Keser, T. Ates, C. Tatar and F. Yakuphanoglu. Controlling of dielectric parameters of insulating hydroxyapatite by simulated body fluid. Materials Science and Engineering: C. 2015;46:118-124. https://doi.org/10.1016/j.msec.2014.10.024.

[10] J. E. Song, N. Tripathy, D. H. Lee, J. H. Park and G. Khang. Quercetin inlaid silk fibroin/hydroxyapatite scaffold promotes enhanced osteogenesis. ACS applied materials & interfaces. 2018;10(39):32955-32964. https://doi.org/10.1021/acsami.8b08119.

[11] L. Forte, P. Torricelli, E. Boanini, M. Gazzano, K. Rubini, M. Fini and A. Bigi. Antioxidant and bone repair properties of quercetin-functionalized hydroxyapatite: An in vitro osteoblast–osteoclast–endothelial cell co-culture study. Acta Biomaterialia. 2016;32:298-308. https://doi.org/10.1016/j.actbio.2015.12.013.

[12] P. N. Silva-Holguín and S. Y. Reyes-López. Synthesis of hydroxyapatite-Ag composite as antimicrobial agent. Dose-Response. 2020;18(3):1559325820951342. https://doi.org/10.1177/1559325820951342.

[13] B. Tang, H. Yuan, L. Cheng, X. Zhou, X. Huang and J. Li. Control of hydroxyapatite crystal growth by gallic acid. Dental Materials Journal. 2015;34(1):108-113. https://doi.org/10.4012/dmj.2014-175.

[14] S. Jerdioui, L. L. Elansari, N. Jaradat, S. Jodeh, K. Azzaoui, B. Hammouti, M. Lakrat, A. Tahani, C. Jama and F. Bentiss. Effects of gallic acid on the nanocrystalline hydroxyapatite formation using the neutralization process. Journal of Trace Elements and Minerals. 2022;2:100009. https://doi.org/10.1016/j.jtemin.2022.100009.

[15] B. Sahin, T. Ates, I. K. Acari, A. A. Barzinjy, B. Ates, İ. Özcan, N. Bulut, S. Keser and O. Kaygili. Tuning electronic properties of hydroxyapatite through controlled doping using zinc, silver, and praseodymium: A density of states and experimental study. Ceramics International. 2024;50(5):7919-7929. https://doi.org/10.1016/j.ceramint.2023.12.120.

[16] E. Landi, A. Tampieri, G. Celotti and S. Sprio. Densification behaviour and mechanisms of synthetic hydroxyapatites.

Journal of the European Ceramic Society. 2000;20(14-15):2377-2387. https://doi.org/10.1016/S0955-2219(00)00154-0.

[17] L. Ibrahimzade, O. Kaygili, S. Dundar, T. Ates, S. V. Dorozhkin, N. Bulut, S. Koytepe, F. Ercan, C. Gürses and A. H. Hssain. Theoretical and experimental characterization of Pr/Ce co-doped hydroxyapatites. Journal of Molecular Structure. 2021;1240:130557. https://doi.org/10.1016/j.molstruc.2021.130557.

[18] F. Baldassarre, A. Altomare, E. Mesto, M. Lacalamita, B. Dida, A. Mele, E. M. Bauer, M. Puzone, E. Tempesta, D. Capelli, D. Siliqi and F. Capitelli. Structural Characterization of Low-Sr-Doped Hydroxyapatite Obtained by Solid-State Synthesis. Crystals. 2023;13(1):117. https://doi.org/10.3390/cryst13010117.

[19] S. C. Ciobanu, S. L. Iconaru, M. V. Predoi, L. Ghegoiu, M. L. Badea, D. Predoi and G. Jiga. Physico-Chemical and Antimicrobial Features of Magnesium Doped Hydroxyapatite Nanoparticles in Polymer Matrix. In Macromolecular Symposia. 2024;413(4):2400022. https://doi.org/10.1002/masy.202400022.

[20] S. Joseph, K. Genasan, U. Anjaneyalu, A. Livingston, S. Samuel and S. Sasikumar. Biomineralization and mechanical studies of sodium substituted hydroxyapatite by a time-saving combustion route. ChemistrySelect. 2023;8(41):e202302660. https://doi.org/10.1002/slct.202302660.

[21] M. S. Hossain and S. Ahmed. FTIR spectrum analysis to predict the crystalline and amorphous phases of hydroxyapatite: a comparison of vibrational motion to reflection. RSC advances. 2023;13(21):14625-14630. https://doi.org/10.1039/D3RA02580B.

[22] O. Kaygili. Combustion synthesis and characterization of Mg-based Fe-doped biphasic calcium phosphate ceramics. Applied Physics A. 2019;125:431. https://doi.org/10.1007/s00339-019-2728-0.

[23] A. A. Korkmaz, L. O. Ahmed, R. O. Kareem, H. Kebiroglu, T. Ates, N. Bulut, O. Kaygili and B. Ates. Theoretical and experimental characterization of Sn-based hydroxyapatites doped with Bi. Journal of the Australian Ceramic Society. 2022;58(3):803-815. https://doi.org/10.1007/s41779-022-00730-5.

[24] U. Anjaneyulu, D. K. Pattanayak and U. Vijayalakshmi. Snail shell derived natural hydroxyapatite: effects on NIH-3T3 cells for orthopedic applications. Materials and Manufacturing Processes. 2016;31(2):206-216. https://doi.org/10.1080/10426914.2015.1070415.

[25] I. Ercan, O. Kaygili, T. Kayed, N. Bulut, H. Tombuloğlu, T. İnce, F. Al Ahmari, H. Kebiroglu, T. Ates, A. Almofleh, F. Firdolas, O. Köysal, E. A. Al-Suhaimi, T. Ghrib, H. Sözeri, M. Yıldız and F. Ercan. Structural, spectroscopic, dielectric, and magnetic properties of Fe/Cu co-doped hydroxyapatites prepared by a wet-chemical method. Physica B: Condensed Matter. 2022;625:413486. https://doi.org/10.1016/j.physb.2021.413486.

[26] F. Ercan, T. S. Kayed, O. Kaygili, N. Bulut, D. Almohazey, T. Ates, F. S. Al-Ahmari, I. Ay, T. Demirci, G. Kirat, T. Flemban, T. İnce, T. Ghrib, E. A. Al-Suhaimi and I. Ercan. Investigation of structural, spectroscopic, dielectric, magnetic, and in vitro biocompatibility properties of Sr/Ni co-doped hydroxyapatites. Ceramics International. 2022;48(18):26585-26607. https://doi.org/10.1016/j.ceramint.2022.05.354.

[27] Y. Ş. Tekin and T. Ates. Comprehensive investigation of the electronic properties of zinc and cobalt doped hydroxyapatite. Journal of the Australian Ceramic Society. 2024;60:1219–1231. https://doi.org/10.1007/s41779-024-01024-8.

[28] S. Mondal, A. Mondal, N. Mandal, B. Mondal, S. S. Mukhopadhyay, A. Dey and S. Singh. Physico-chemical characterization and biological response of Labeo rohita-derived hydroxyapatite scaffold. Bioprocess and Biosystems Engineering. 2014;37:1233–1240. https://doi.org/10.1007/s00449-013-1095-z.